

Universal profile of dark matter halos and the spherical infall model

Ewa L. Łokas

Copernicus Astronomical Center, Bartycka 18, 00–716 Warsaw, Poland

16 January 2018

ABSTRACT

I propose a modification of the spherical infall model for the evolution of density fluctuations with initially Gaussian probability distribution and scale-free power spectra in Einstein-de Sitter universe as developed by Hoffman & Shaham. I introduce a generalized form of the initial density distribution around an overdense region and cut it off at half the inter-peak separation accounting in this way for the presence of the neighbouring fluctuations. Contrary to the original predictions of Hoffman & Shaham the resulting density profiles within virial radii no longer have power-law shape but their steepness increases with distance. The profiles of halos of galactic mass are well fitted by the universal profile formula of changing slope obtained as a result of N -body simulations by Navarro, Frenk & White. The trend of steeper profiles for smaller masses and higher spectral indices is also reproduced. The agreement between the model and simulations is better for smaller masses and lower spectral indices which suggests that galaxies form mainly by accretion while formation of clusters involves merging.

Key words: methods: analytical – cosmology: theory – galaxies: clustering – galaxies: formation – large-scale structure of Universe

1 INTRODUCTION

It is generally believed that the structure in the universe emerged hierarchically from initially small density fluctuations. Small fluctuations, which at present remain such only at very large smoothing scales, can be successfully described by the linear theory. On smaller scales however, nonlinear effects come into play and linear approximation is no longer valid. In the weakly nonlinear regime perturbative approach proved extremely successful in predicting the statistical properties of density fields at scales exceeding $10 h^{-1}$ Mpc. In order to predict properties of single objects we must however trace the evolution of density up to strongly nonlinear regime. The price to pay is high: we have to restrict the analysis to one object neglecting its interactions with the neighbourhood.

The simplest deterministic model of strongly nonlinear evolution proposed by Gunn & Gott (1972), called the spherical model, described the behaviour of a uniformly overdense region in the otherwise unperturbed, expanding Universe. It was extended by Gott (1975) and Gunn (1977) to apply to the evolution of matter around an already collapsed density perturbation superposed on a homogeneous background. The main prediction of the model (called the spherical accretion or the secondary infall model, hereafter

SIM) was that the matter collapsing around the perturbation should form a halo with $r^{-9/4}$ density profile.

It is much more realistic to assume that the progenitors of structure were not the collapsed perturbations but the local maxima (rare events) in the density field which had initially Gaussian probability distribution. This was the approach of Hoffman & Shaham (1985, hereafter HS) who applied SIM to the hierarchical clustering scenario. They assumed that the density peak dominates to some extent the surroundings causing the collapse of the material that is gravitationally bound to it. The initial density profile around the peak was approximated by the mean density predicted by the initial probability distribution which was assumed to be Gaussian. HS considered scale-free initial power spectra of fluctuations in different cosmologies and found that the final profiles of halos steepen for higher spectral indices and lower density parameter Ω_0 .

This kind of dependence on cosmological parameters was confirmed via the results of completely different approach to studies of structure formation: the N -body simulations. Quinn, Salmon & Zurek (1986), Efstathiou et al. (1988) and more recently Crone, Evrard & Richstone (1994) among others confirmed the analytical predictions by fitting power laws to the density profiles of dark matter halos resulting from their simulations.

Recently Navarro, Frenk & White (1997, hereafter

NFW) performed a series of high-resolution N -body simulations for power-law initial spectra and found that the density profiles of dark halos in large range of masses can be fitted with a simple formula with only one fitting parameter. The density profile was observed to steepen from r^{-1} near the centre of the halo to r^{-3} at large distances. This confirmed earlier results of these authors obtained for CDM cosmologies. Similar shapes of profiles were also observed by Cole & Lacey (1996) and Tormen, Bouchet & White (1997) in their N -body simulations.

Although the overall trend of steeper profiles for higher spectral indices and lower Ω_0 predicted by SIM was confirmed, NFW claim that the changing slope of the profile is “at odds with the analytic predictions”. In fact this is only true in the case of $\Omega_0 = 1$ for which SIM indeed predicts a power-law profile. However, for large (i.e. close to 1) values of Ω_0 SIM in the form proposed by HS is least reliable. This is mainly due to the fact that SIM describes the evolution of a single overdense region while in reality the halos forming at various locations compete for mass. As a result, the mass accreted by an overdense region is not the whole mass which is gravitationally bound to it (in the case of $\Omega_0 = 1$ this mass is infinite). Another limitation of SIM comes from the statistical approach applied in determining the initial conditions: the initial density distribution has a finite coherence scale which also may influence the amount of mass accreted onto the peak.

The paper is organized as follows: after a short presentation of SIM in Section 2, in Section 3 and 4 I outline proposed modifications to the model and in Section 5 compare obtained halo density profiles to the results of N -body simulations. The discussion follows in Section 6.

2 THE STANDARD SPHERICAL INFALL MODEL FOR $\Omega = 1$

In the following I present the main assumptions and results of SIM as applied to the density contrast field with initially Gaussian probability distribution. This version of the model was first presented for the case of linear fields by HS and slightly modified by Lokas (1998) in attempt to take into account the weakly nonlinear corrections. In the following only the linear approximation will be used to determine initial conditions. The remaining assumptions and conventions will follow those of Lokas (1998) except for a change in notation introduced in order to conform to the widely accepted notation for the parameters of the universal profile.

I will consider the Einstein-de Sitter cosmological model with $\Omega = 1$ and zero cosmological constant. The initial probability distribution of the density field will be assumed to be Gaussian. The initial density power spectrum will be modeled by the scale-free form

$$P(k) = Ck^n \quad (1)$$

with indices $n = -1.5, -1, -0.5, 0$ which are of biggest cosmological interest. The fields will be smoothed with a filter of a Gaussian shape

$$W_G(kR) = e^{-k^2 R^2/2}. \quad (2)$$

For such spectra and smoothing the density field can be characterized by the correlation coefficient

$$\varrho = \frac{\xi_R(r)}{\sigma^2} = {}_1F_1\left(\frac{n+3}{2}, \frac{3}{2}, -\frac{x^2}{4}\right) \quad (3)$$

where $\xi_R(r)$ is the (auto)correlation function of the two values of the density fields (smoothed at comoving scale R) at points separated by distance r , x is the distance in units of R : $x = r/R$ and σ is the linear rms fluctuation at scale R which in this case is given by

$$\sigma^2 = CD^2(t) \frac{\Gamma[(n+3)/2]}{(2\pi)^2 R^{n+3}} \quad (4)$$

where the time dependence is

$$D(t) = \frac{1}{1+z}. \quad (5)$$

Let us assume that at $r = 0$ we detect an overdense region of density equal to a standard deviations: $\delta(r = 0) = a\sigma$ (for high enough a this is approximately equivalent to assuming there is a peak at $r = 0$). Two-point probability distribution function then predicts that at distance r (or x if we measure the distance in units of R) the expected density contrast is

$$\langle \delta(x) \rangle = \varrho(x) a\sigma \quad (6)$$

with $\varrho(x)$ given by equation (3).

The dynamical evolution of matter at the distance x_i from the peak is determined by the mean cumulative density perturbation within x_i which is given by

$$\Delta_i(x_i) = \frac{3}{x_i^3} \int_0^{x_i} \delta(x) x^2 dx. \quad (7)$$

If we assume that $\delta(x) = \langle \delta(x) \rangle$ the expected cumulative density can be approximated by

$$\langle \Delta_i(x_i) \rangle = \begin{cases} a\sigma & \text{for } x_i \ll 1 \\ a\sigma h(n) x_i^{-(n+3)} & \text{for } x_i \gg 1. \end{cases} \quad (8)$$

The values of the numerical factor $h(n)$ can be found in Lokas (1998). A similar approximation for large x_i was used by HS as the initial condition for their SIM. The approximation at large x_i in the form given above is accurate to within 10% for $x_i \geq 5$.

The cumulative density contrast $\Delta_i(x_i)$ describes the initial density distribution around the peak. Assuming that the cumulative density can be approximated by the mean, $\Delta_i(x_i) = \langle \Delta_i(x_i) \rangle$, SIM can be used to predict the final density profile which will form after shells which are bound to the peak collapse onto it. The distance to the farthest shell which is bound to collapse is given by the condition of the vanishing energy

$$\Delta_i(x_{i,0}) = \Omega_i^{-1} - 1 = 0 \quad (9)$$

where Ω_i is the density parameter at some initial epoch at which we specify the initial density distribution. In the case of $\Omega = 1$ the scale $x_{i,0}$ of the gravitational influence of any overdense region is infinite, the region should therefore collect mass from the whole universe.

According to SIM after virialization the shell x_i ends up at $x = fx_m$ where x_m is the maximum radius given by

$$x_m = x_i \frac{\Delta_i + 1}{\Delta_i} \quad (10)$$

and f is the collapse factor, which in the case of scale free

initial conditions for large x_i , equation (8), can be approximated by a constant of the order of 1/2 (see Zaroubi & Hoffman 1993). The final density profile then follows from the conservation of mass

$$\rho(x)x^2dx = \rho_i(x_i)x_i^2dx_i. \quad (11)$$

If we approximate the initial density of the shell of radius x_i

$$\rho_i(x_i) = \rho_{b,i}[1 + \delta_i(x_i)] \quad (12)$$

by the background (critical) density $\rho_{b,i} = \rho_{\text{crit},i} = (1 + z_i)^3 \rho_{\text{crit},0}$ and expand the right hand side of equation (10) in Δ_i keeping only the linear term, we will end up with the power law density profile found by HS

$$\frac{\rho(x)}{\rho_{\text{crit},0}} = \frac{(1 + z_i)^3}{n + 4} \left(\frac{a\sigma h}{f} \right)^{3/(n+4)} x^{-3(n+3)/(n+4)}. \quad (13)$$

The density profiles will be expressed here as above in units of the present critical density to ensure direct comparison with the results of N -body simulations.

It is interesting to note that what is usually quoted as the prediction of SIM for hierarchical clustering scenarios is the special case (13) which is valid only for $\Omega = 1$. In the case of open universe the slope of the halo steepens gently with the distance from the centre starting with the slope (13) near the centre and approaching x^{-4} for shells close to the last bound shell. The case of $\Omega < 1$ will be treated in the follow-up paper.

3 HOW TO IMPROVE THE SPHERICAL INFALL MODEL?

The main and most questionable assumptions underlying SIM as formulated by HS are of course the spherical symmetry of the problem and the absence of peculiar velocities. I will keep the assumptions here and show that even with these simplifications the agreement between the model and the results of N -body simulations can be improved.

First I propose to relinquish the large x_i approximation for the $\langle \Delta_i(x_i) \rangle$, equation (8) applied by HS in their calculations. The general formula for the expected cumulative density contrast can be found using equations (3), (6) and (7)

$$\begin{aligned} \langle \Delta_i(x_i) \rangle &= \frac{6a\sigma}{(n+1)x_i^2} \left[{}_1F_1 \left(\frac{n+1}{2}, \frac{3}{2}, -\frac{x_i^2}{4} \right) \right. \\ &\quad \left. - {}_1F_1 \left(\frac{n+1}{2}, \frac{1}{2}, -\frac{x_i^2}{4} \right) \right]. \end{aligned} \quad (14)$$

The main reason for this generalization is that especially with the conditions given below the main contribution to the final density profile of the halo comes from x_i of the order of few. Although HS used the large x_i approximation as the one applicable at large distances from the peak, it is possible to interpret large x_i also as small smoothing scales. The smoothing procedure of the initial density field that is performed here in order to determine the location of the overdense regions has no equivalent in real structure formation or N -body simulations where the only artificial scales are those of softening length and the size of the simulation box. One may argue that the large distance (or small smoothing scale) approximation to $\langle \Delta_i(x_i) \rangle$ is therefore more realistic.

Table 1. The values of the scales of influence $x_{i,\text{COH}}$ and $x_{i,\text{pp}}/2$ for peaks of height $a = 3$ for different spectral indices n .

n	$x_{i,\text{COH}}$	$x_{i,\text{pp}}/2$
-1.5	14.3	7.36
-1.0	9.02	6.45
-0.5	6.66	5.81
0.0	5.35	5.32

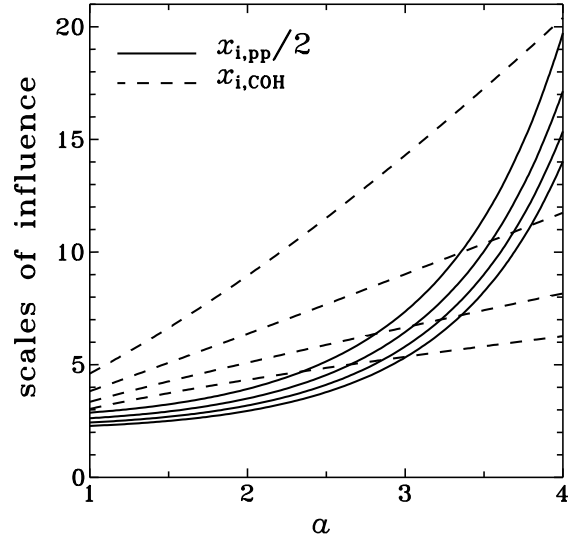


Figure 1. The scale of coherence $x_{i,\text{COH}}$ (dashed lines) and half the distance between peaks $x_{i,\text{pp}}/2$ (solid lines) as functions of the height of the peak a for different spectral indices. The four curves in each set correspond from top to bottom to $n = -1.5, -1, -0.5$ and $n = 0$.

However, taking into account the intrinsic role of the initial smoothing in determination of the initial conditions for collapse, the masses of halos etc. it is difficult to accept such argument.

Another limitation of the model presented in Section 2 comes from the statistical approach to determining the initial conditions for collapse. The density profile is evaluated with the assumption $\Delta_i(x_i) = \langle \Delta_i(x_i) \rangle$, while this approximation can only be considered valid for scales up to the scale of coherence $x_{i,\text{COH}}$ defined by

$$\langle \Delta_i \rangle = \Sigma_\Delta. \quad (15)$$

The calculation of the dispersion Σ_Δ in the case of power-law spectra and Gaussian smoothing is presented in Appendix A. Equation (15) can be then solved numerically for $x_{i,\text{COH}}$. The results for different spectral indices n and heights of the peak a are shown in Figure 1. Table 1 lists the values of $x_{i,\text{COH}}$ for the peak of height $a = 3$ that will be considered in the calculation of the profiles.

Similar calculations, but without providing the analytical expressions for $\langle \Delta_i \rangle$ and Σ_Δ , were performed by HS and also by Peebles (1984) and Ryden (1988) who considered peaks instead of overdense regions. HS and Ryden (1988)

then consider the fraction of mass subscribed to peaks higher than $a\sigma$ in the case of different power spectra

$$F(>a) = \frac{4\pi}{3} \int_a^\infty [r_{i,COH}(\nu)]^3 N_{pk}(\nu) d\nu \quad (16)$$

where $N_{pk}(\nu)$ is the differential number density of peaks given by equations (4.3)-(4.10b) of Bardeen et al. (1986, hereafter BBKS). Since $r_{i,COH}(\nu)$ grows faster with ν for lower spectral indices, for example $F(>3)$ is below unity for higher spectral indices to a few for lower spectral indices. This leads HS to assume that the most probable peaks around which structure will form are those for which $F(>a) = 1$. However, this way they end up with a rather surprising value of $a > 4$ for the height of the most probable peak for $n = -2$. From the statistics of peaks by BBKS we know that $N_{pk}(\nu)$ is a strongly decreasing function for large ν and peaks with $a > 4$ are very rare.

I propose here to consider the distance between peaks as an additional constraint on the cumulative density distribution around a peak. It is reasonable to assume that only the peaks higher than a should be considered as “dangerous” for the structure forming around our chosen peak. Since the number density of peaks higher than a for sufficiently high values of a ($a = 2, 3, 4$) is a strongly decreasing function of a , we may assume that the peaks nearest to our peak are of height close to a . The scales of influence of our peak and the neighbouring one will be similar and we may approximate this scale as half the distance between peaks, $x_{i,pp}/2$. The scale $x_{i,pp}$ is determined by the number density of peaks higher than a :

$$x_{i,pp} = \frac{[n_{pk}(>a)]^{-1/3}}{R} \quad (17)$$

where

$$n_{pk}(>a) = \int_a^\infty N_{pk}(\nu) d\nu. \quad (18)$$

The numerical results for $x_{i,pp}/2$ for different spectral indices are shown in Figure 1. The results for $a = 3$ are also listed in Table 1. In the following I will simulate the constraints on the cumulative density (14) by cutting it off at the smaller of the two scales $x_{i,pp}/2$ and $x_{i,COH}$. I have chosen to consider here peaks of given height $a = 3$ which are high enough to collapse by themselves and frequent enough to produce large number of objects. We see that the scale $x_{i,pp}/2$ for $a = 3$ is always smaller than the corresponding $x_{i,COH}$ except for the highest spectral index considered, $n = 0$, where the two scales are almost equal. This motivates the introduction of the cut-off at $x_{i,pp}/2$ and not $x_{i,COH}$.

The remaining issue is the shape of the cut-off function. I will adopt a sharp cut-off such that the corrected cumulative density will be

$$\Delta_{i,cut}(x_i) = \frac{\langle \Delta_i(x_i) \rangle}{1 + e^{(x_i - x_{i,pp}/2)/w}} \quad (19)$$

with $\langle \Delta_i(x_i) \rangle$ given by equation (14). Unfortunately, in contrast to the problem of the scale of cut-off, we cannot predict the width of the filter, w from the model. It will be treated as an unknown parameter which has to be specified by matching the results from SIM and N -body simulations (see Section 5).

Summarizing, the final density profile of the virialized halo is given by

$$\frac{\rho(x)}{\rho_{crit,0}} = (1 + a\sigma\varrho)(1 + z_i)^3 \left(\frac{x_i}{x} \right)^2 \frac{dx_i}{dx} \quad (20)$$

with

$$x = \frac{x_i f[\Delta_{i,cut}(x_i) + 1]}{\Delta_{i,cut}(x_i)}. \quad (21)$$

Formula (20) gives a complicated but analytical expression for the density profile as a function of the initial radius x_i which is related to the final radius x by equation (21). Since the initial density distribution in its generalized form (14) is not scale free the collapse factor f in equation (21) can no longer be assumed to be the same constant for all shells (for the results with $f = 1/2$ see Lokas 1999). Detailed calculation of this factor is presented in the following section.

4 THE COLLAPSE FACTOR

The purpose of this section is to find a correction to the fiducial density profile defined as the density distribution with all shells stopping at their maximal radii. This corresponds to putting $f = 1$ in equations (20)-(21). In reality after reaching the maximum radius a given shell will start oscillating and it will contribute to the actual mass contained inside inner shells which are expected to contract adiabatically (see the discussion in Zaroubi & Hoffman 1993) by a factor

$$f(x_i) = \frac{M(x_i)}{M(x_i) + m_{add}(x_i)} \quad (22)$$

where $M(x_i) = M(x)$ is the mass contained inside the shell of radius x_i or x and $m_{add}(x_i)$ is the mass contributed by the outer shells.

If the shape of the fiducial profile is a power-law given by (13) the collapse factor is easily determined to be

$$f = \frac{1}{1 + (3 - \gamma) \int_1^U u^{2-\gamma} P(1/u) du} \quad (23)$$

where $\gamma = 3(n+3)/(n+4)$, U is the size of the system in units of the radius of the considered shell, P is the fraction of time a particle belonging to shell of radius x' spends within radius x

$$P(x, x') \propto \int_0^x \frac{dx}{v}. \quad (24)$$

In the case of scale-free profile P can be expressed as a function of a single variable $u = x/x'$. The normalization of P is provided by the obvious condition $P(x, x' = x) = 1$. The velocity v is calculated by integrating the equation of motion of the shell $d^2r/dt^2 = -GM/r^2$.

In the scale-free case it is possible to obtain analytical solutions for P

$$\begin{aligned} P(u) &= \frac{\gamma\Gamma[\gamma/(4-2\gamma)]u}{2\sqrt{\pi}\Gamma[1/(2-\gamma)]} \\ &\times {}_2F_1\left[\frac{1}{2}, \frac{1}{2-\gamma}, 1 + \frac{1}{2-\gamma}, u^{2-\gamma}\right] \end{aligned} \quad (25)$$

for $\gamma < 2$ and

$$\begin{aligned} P(u) &= \frac{2\Gamma[1/(\gamma-2)]u^{\gamma/2}}{\sqrt{\pi}\gamma\Gamma[\gamma/(2\gamma-4)]} \\ &\times {}_2F_1\left[\frac{1}{2}, \frac{\gamma}{2\gamma-4}, 1 + \frac{\gamma}{2\gamma-4}, u^{\gamma-2}\right] \end{aligned} \quad (26)$$

for $\gamma > 2$. These results provide generalizations of the limiting cases considered by Zaroubi & Hoffman (1993). The collapse factor can then be evaluated numerically for any γ and U .

When the fiducial density profile is scale-dependent as in the case of interest here the calculation of P and m_{add} is more complicated and has to be done numerically. The velocity in equation (24) is

$$v \propto [E(x') - E(x)]^{1/2} \quad (27)$$

where

$$E(x) \propto \int \frac{M(x)}{x^2} dx = \int \frac{x_i \Delta_i^2}{1 + \Delta_i} \frac{dx}{dx_i} dx_i \quad (28)$$

where we used the expression for mass within x_i

$$M(x) = M(x_i) = \frac{4\pi}{3} \rho_{\text{crit},0}(x_i R)^3 [1 + \Delta_i(x_i)] \quad (29)$$

and equation (21) with $f = 1$. The cumulative density distribution Δ_i is taken in generalized form with cut-off, equation (19).

Due to the complicated form of the integrand in the expression (28) for E the integration cannot be performed analytically, but the integrand can be exactly approximated by a polynomial in x_i making the integration possible. After changing variables from x to x_i in equation (24) the value of P can be calculated numerically for any (x_i, x'_i) pair. The added mass in equation (22) can then be obtained by summing up the input from j intervals between a given shell and the shell that is presently turning around $x_{i,ta}$ (the turn-around radius is obtained in a similar way as the virial radius $x_{i,v}$, from $t_u = t_{\text{coll}}/2$, see the next Section)

$$m_{\text{add}}(x_i) = 4\pi \rho_{\text{crit},0} R^3 (1 + z_i)^3 \sum_j \int_{x_{i,j}}^{x_{i,j+1}} y_i^2 [1 + \delta_i(y_i)] \times P\left(x_i, \frac{x_{i,j} + x_{i,j+1}}{2}\right) dy_i. \quad (30)$$

The result for f is sensitive to the number of steps taken in the integration but usually $j = 10$ is enough to obtain f with two digit accuracy for $x_i > 1$.

After calculating the factor f for a number of x_i values we can approximate the function $f(x_i)$ by a polynomial in x_i and introduce it into equation (21). From equation (20) we will then obtain the final density profile of a halo.

5 COMPARISON WITH THE UNIVERSAL PROFILE

NFW performed a series of N -body simulations of structure formation in flat and open universe for different scale-free power spectra of the form (1). They concluded that the density profiles of dark matter halos are well fitted in all cases by a formula

$$\frac{\rho(x)}{\rho_{\text{crit},0}} = \frac{\delta_{\text{char}}}{(r/r_s)(1 + r/r_s)^2} \quad (31)$$

with a single fitting parameter δ_{char} , the characteristic density. The so-called scale radius r_s is defined by

$$r_s = \frac{r_v}{c} \quad (32)$$

where r_v is the virial radius i.e. the distance from the centre of the halo within which the mean density is v times the critical density. c in equation (32) is the so-called concentration parameter, which is related to the characteristic density by

$$\delta_{\text{char}} = \frac{vc^3}{3[\ln(1 + c) - c/(1 + c)]}. \quad (33)$$

NFW assume $v = 200$ for all considered cosmological models, which is not strictly correct. For $\Omega = 1$ the exact prediction of the spherical model for the ratio of the density to the critical density for objects collapsing at the present epoch is $v = 18\pi^2 \approx 178$ (see e.g. Lacey & Cole 1993) so the natural choice would seem to adopt the value $v = 200$ in order to keep the assumptions as close as possible to those of NFW. However, this value is inconsistent with the more advanced SIM considered here: the value of v can be calculated and it proves to be much lower than 200: it is of the order of 30 for the small masses and reaches 200 only for the largest halos. Fitting the NFW formula with $v = 200$ to the results of SIM produces a significant offset between the fit and the SIM results, one therefore has to adopt the true value of v . Then the problem of comparison with the simulations arises: what is the relation between masses of halos determined from simulations with different v ? Fortunately, at the virial radii the density profiles of halos in the simulations have slope -3 so the mass grows very slowly (logarithmically) with r and the masses determined with $v = 200$ and $v = 30$ should be almost the same.

Since the measurements of the halo density profiles in the N -body simulations of NFW are all done at the final epoch which is identified with the present, in the following I will assume that for all the halos the collapse time is the present epoch. According to the spherical model the collapse time of the shell x_i in the $\Omega = 1$ universe is (Padmanabhan 1993)

$$t_{\text{coll}} = \frac{\pi(1 + \Delta_i)}{H_0(1 + z_i)^{3/2} \Delta_i^{3/2}}. \quad (34)$$

The present age of the universe is $t_u = 2/(3H_0)$ and solving equation $t_{\text{coll}} = t_u$ for Δ_i gives us the values of the cumulative density contrast as a function of z_i , which will be denoted by $\Delta_{i,v}$. This density contrast corresponds to the presently collapsing initial shell $x_{i,v}$ which can then be found by numerically solving equation

$$\Delta_{i,\text{cut}}(x_i) = \Delta_{i,v}, \quad (35)$$

and the corresponding final virial radius x_v is obtained from equation (21). In order to solve this equation we have to specify the initial conditions: the height of the peak a and the rms fluctuation of the density field σ . I have already chosen $a = 3$ and will assume that for all halos the starting point is such that $a\sigma = 0.1$, small enough for the linear theory to be valid. Final results are not very sensitive to this particular choice.

We also need to make connection to the present magnitude of fluctuations so I will adopt the standard normalization of the density field such that $\sigma_8 = 1$ (rms fluctuation in spheres of radius $8h^{-1}$ Mpc is one). This normalization can be also expressed in terms of the present nonlinear mass M_* used by NFW. This mass is defined by the condition of the rms fluctuation at this mass scale being equal to the present

critical threshold for collapse δ_{crit} . Given the dependence of σ on the smoothing scale this yields

$$M_* = M(R) \left[\frac{\sigma_{\text{TH}}(R)}{\delta_{\text{crit}}} \right]^{6/(n+3)} \quad (36)$$

where R is the smoothing scale used for normalization, subscript TH refers to the top-hat smoothing, equation (A7), and $M(R) = 4\pi R^3 \rho_b/3$. For $\Omega = 1$ the threshold is $\delta_{\text{crit}} = 1.69$ so with our normalization at $R = 8h^{-1}$ Mpc we have

$$M_* = 5.96 (1.69)^{-6/(n+3)} \times 10^{14} h^{-1} M_\odot. \quad (37)$$

Once the normalization is set and the conditions $a = 3$ and $a\sigma = 0.1$ are adopted choosing the initial redshift z_i for a given spectral index n gives us the comoving smoothing scale R with which the overdense regions are identified. The mass of the halo within the virial radius x_v can then also be determined. According to the results of the previous section the total mass inside the virial radius is

$$M = M(x_{i,v}) + m_{\text{add}}(x_{i,v}). \quad (38)$$

One of the main results of NFW was the dependence of the shape of the density profiles of halos on their mass: their profiles were steeper for lower masses. On the other hand, the standard prediction of SIM, equation (13), gives the same profile independently of mass. However, with the improvements introduced in Section 3 and 4 it is possible to reproduce the dependence of the profiles on mass.

It has been suggested in the literature (e.g. Katz, Quinn & Gelb 1993) that N -body simulations indicate that if the density field is smoothed with one scale R lower peaks end up as galaxies and higher ones as clusters. This, however, would violate the hierarchical way of structure formation since higher peaks collapse earlier. Another argument against such assumption comes from the calculations based on the improved SIM for $n = -1$: the reasonable range of peak heights a between 2 and 4, which are most likely to produce halos, leads for a given smoothing scale to the range of masses spanning only one order of magnitude, while in N -body simulations NFW observe halos with masses spanning few orders of magnitude. This suggests that the dependence on mass should rather be related to the initial smoothing scale.

Calculations show that the mass of a halo increases with the smoothing scale up to the scale for which the solution of equation (35) yields rather small values of $x_{i,v}$ (of the order of unity). In these cases only the nearest neighbourhood of the peak determined with the smoothing scale R managed to collapse by the present. Such peaks cannot be considered as collapsed structures because they accreted up till now only a small fraction of the mass that is bound to them (i.e. contained inside the cut-off scale). Therefore in the following I will deal only with objects that have mass increasing with the smoothing scale. For clarity hereafter I will consider different smoothing scales for only one height of the peak $a = 3$.

NFW suggest that the dependence of the shape of the halo on its mass is related to the formation time of the halo: smaller halos that formed earlier have steeper profiles. Although I have assumed the collapse time to be the present epoch for all halos, this faster collapse of smaller halos can nevertheless be observed: smaller masses are obtained from

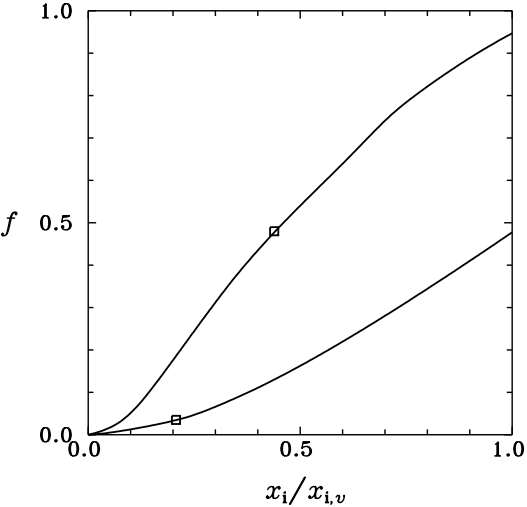


Figure 2. The collapse factor f as a function of the initial radius of a shell (in units of the virial radius) for spectral index $n = -1$. The upper and lower curves correspond respectively to the small and large mass.

smaller smoothing scales which correspond to higher initial redshifts z_i and from equation (34) we have that constant collapse time leads to lower Δ_i and therefore higher $x_{i,v}$. Smaller halos form earlier in the sense that their initial redshifts are higher and by the present epoch their virial radii $x_{i,v}$ reach the cut-off scale.

Given the initial conditions as specified above we may now proceed to the direct comparison of the profiles obtained from SIM and the simulations. An important step in determination of SIM profiles is the calculation of the collapse factor (see Section 4). Figure 2 shows the dependence of this factor on the initial radius of the shell for two different masses in the case of $n = -1$. The upper curve in the figure corresponds to the smallest mass available for $n = -1$ (with $z_i = 1500$), i.e. $0.0017M_* = 2.1 \times 10^{11} h^{-1} M_\odot$. The lower curve is for the largest mass (with $z_i = 43$), $3.3M_* = 4.1 \times 10^{14} h^{-1} M_\odot$. Note that the initial radius was expressed in units of the initial virial radius $x_{i,v}$, which is much larger for the smaller mass. The squares marked in the plot show the points corresponding to $0.01x_v$. Since the density profiles will be considered in the range $0.01x_v < x < x_v$, only the collapse factor values to the right of the marked points will be taken into account in the calculations.

The behaviour of the collapse factor confirms the intuition one may obtain from the scale-free case, equations (23)-(26): the collapse factor is smaller for higher effective index of the cumulative density distribution (see the discussion in Zaroubi & Hoffman 1993). Near the center of the halo, where the initial density distribution is flat, the outer shells contribute significantly to the inner mass and the contraction is stronger. In more steeper parts of the density distribution the outer shells contribute less and contraction is weaker. The dependence on mass comes from the fact that small mass halos have large virial radii $x_{i,v}$ reaching steeper parts of the distribution and even the cut-off scale, while in large mass halos the final density distribution comes from shells that initially were quite close to the peak.

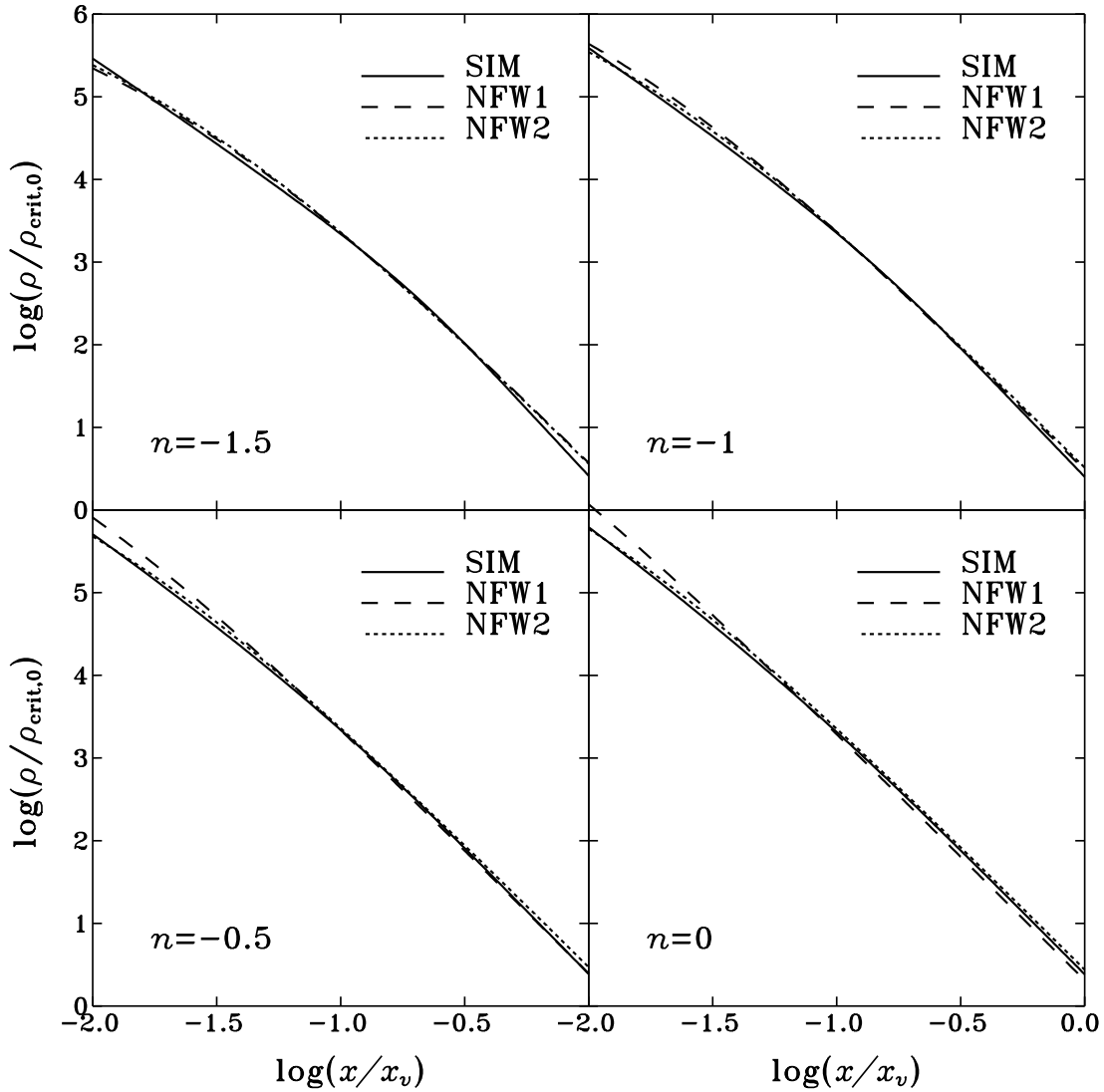


Figure 3. The density profiles of dark matter halos of mass of the order of $0.02M_*$ for different spectral indices n in the range $0.01x_v < x < x_v$. The solid lines show the predictions of SIM. The long-dashed ones give the NFW results with their fitted concentrations, while the short-dashed curves present the NFW formula (39) with concentrations fitted to SIM results.

Table 2. The parameters characterizing the small mass halos whose density profiles are presented in Figure 3.

n	z_i	$\Delta_{i,v}$	$R[h^{-1} \text{ Mpc}]$	$x_{i,v}$	x_v	$r_v[h^{-1} \text{ Mpc}]$	$M[10^{12}h^{-1}M_\odot]$	M/M_*	c_{NFW1}	c_{NFW2}
-1.5	350	0.00805	0.142	7.54	879	0.356	1.55	0.0211	31.0	33.5
-1.0	600	0.00469	0.188	6.76	1348	0.422	2.58	0.0208	59.2	46.9
-0.5	1000	0.00281	0.226	6.21	2065	0.466	3.45	0.0203	131	65.7
0.0	1500	0.00187	0.268	5.73	2861	0.511	4.53	0.0212	306	84.4

Table 3. The parameters characterizing the large mass halos whose density profiles are presented in Figure 4.

n	z_i	$\Delta_{i,v}$	$R[h^{-1} \text{ Mpc}]$	$x_{i,v}$	x_v	$r_v[h^{-1} \text{ Mpc}]$	$M[10^{13}h^{-1}M_\odot]$	M/M_*	c_{NFW1}	c_{NFW2}
-1.5	150	0.0188	0.438	6.50	301	0.872	3.18	0.432	15.6	14.0
-1.0	180	0.0157	0.625	5.45	298	1.03	5.55	0.447	21.6	15.1
-0.5	200	0.0141	0.816	4.67	280	1.14	7.83	0.461	34.9	16.2
0.0	200	0.0141	1.02	4.01	240	1.22	9.83	0.470	62.0	16.8

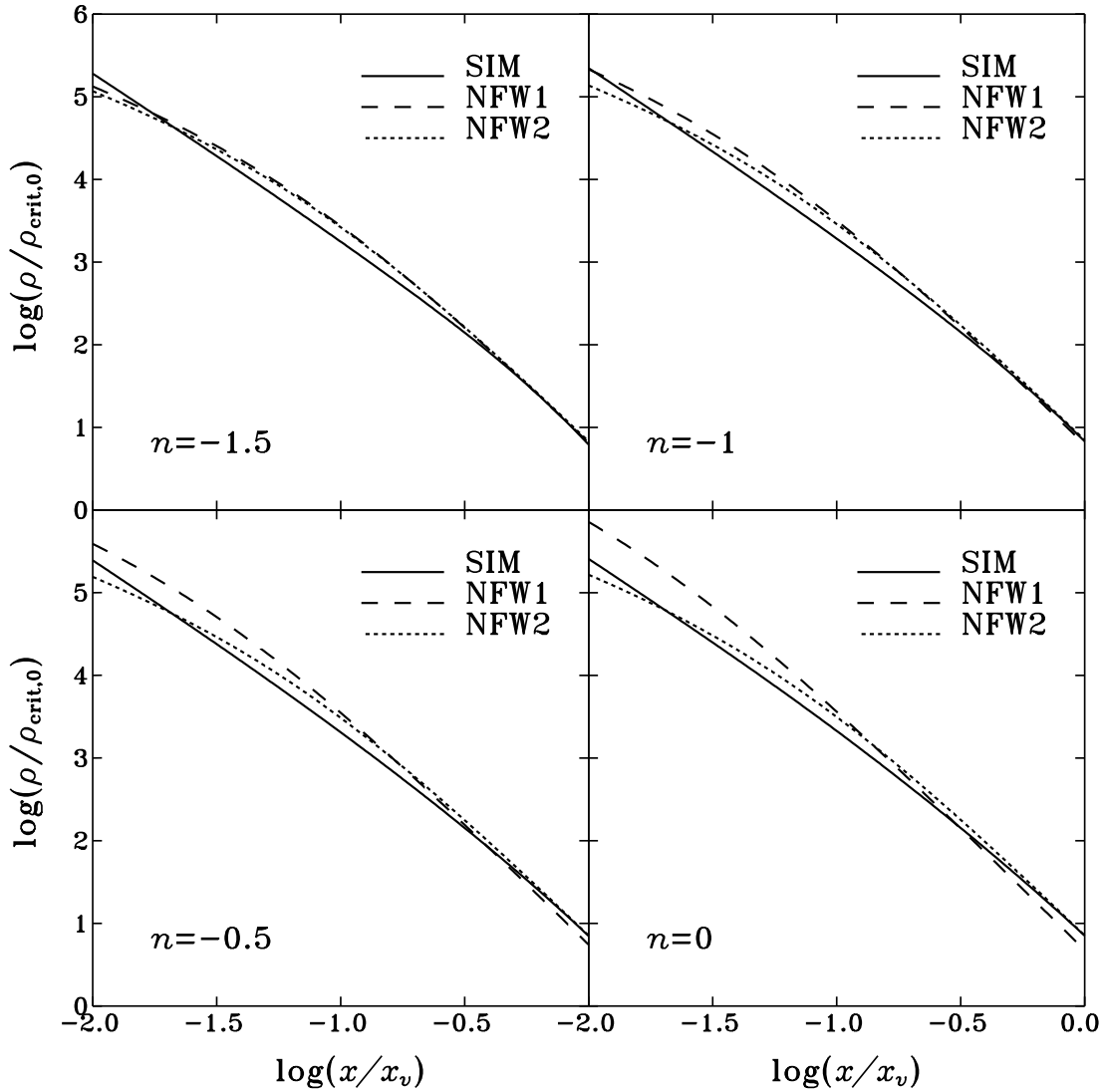


Figure 4. The same as Figure 3 but for masses of the order of $0.5M_*$.

In the comparison between the density profiles predicted by SIM to the results of the *N*-body simulations of NFW I will use the NFW formula (31) in the form

$$\frac{\rho(x)}{\rho_{\text{crit},0}} = \frac{vc^3}{3[\ln(1+c) - c/(1+c)](cx/x_v)(1+cx/x_v)^2} \quad (39)$$

where definition of characteristic density (33) was used and the distances were expressed in units of the smoothing radius and denoted by x in order to provide direct correspondence with the predictions of SIM. NFW claim that their fitting formula is valid in the range $0.01x_v < x < x_v$. I therefore fit the formula (39) to the points $(x, \rho/\rho_{\text{crit},0})$ obtained from equations (20)-(21), spaced uniformly in $\log(x/x_v)$ in this range. For a given spectral index n the single fitting parameter is the concentration c .

NFW consider density profiles of halos of mass roughly in the range $0.01 < M/M_* < 10$ so the initial redshifts will be chosen here so as to obtain similar range of masses. Examples of profiles for halos of different mass are shown

in Figures 3 and 4. Figure 3 shows the density profiles for objects of mass of the order of $0.02M_*$, which corresponds to a big galaxy mass scale, while Figure 4 shows the profiles for halos of mass of the order of $0.5M_*$, which is closer to the mass of a galaxy cluster. Such choice of the mass values is motivated by the range of masses obtained for different spectral indices (see Figure 5 and the following discussion). The initial redshifts needed to obtain halos of those masses and all the following parameters are given in Tables 2 and 3 for the small and large masses respectively.

In agreement with the above discussion of the dependence of mass on the smoothing scale, smaller masses require smaller smoothing scales and the condition $a\sigma = 0.1$ translates into their larger initial redshifts z_i . In the case of small masses the initial virial radii $x_{i,v}$ are of the order of the cut-off scale $x_{i,pp}/2$ which means that the cut-off really influences the formation of small halos, i.e. in the absence of the cut-off their virial radii would be much larger. In the case of the large mass halos the situation is different: their virial

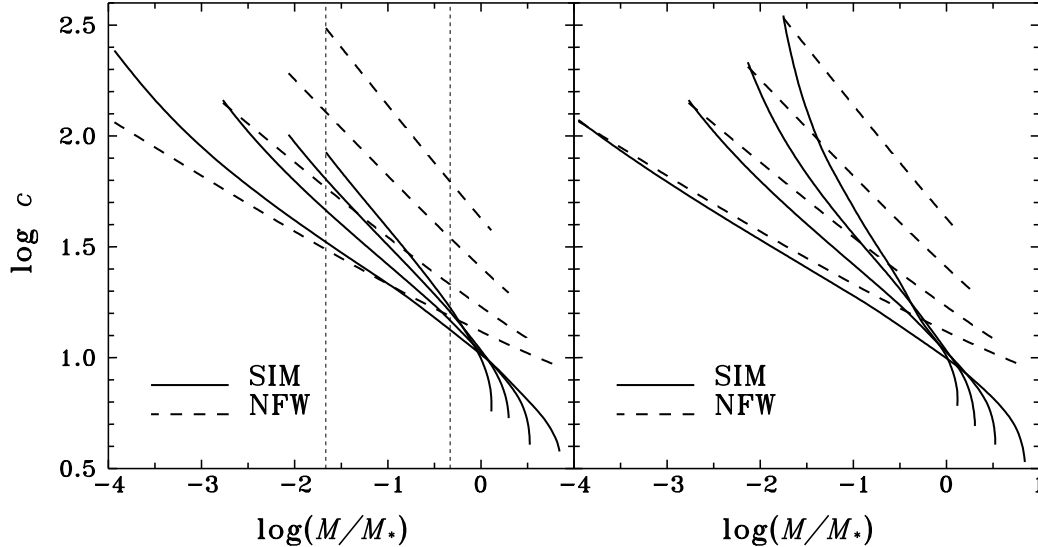


Figure 5. The dependence of the concentration parameter c on the mass. The dashed lines show the results of N -body simulations of NFW, and the solid curves represent the results of SIM. In each set the curves from top to bottom correspond to $n = 0, -0.5, -1$ and -1.5 respectively. In the left panel the SIM results were obtained with constant $w = 0.6$ while in the right panel the values were $w = 0.14, 0.31, 0.6, 0.95$ respectively for $n = 0, -0.5, -1$ and -1.5 .

radii $x_{i,v}$ are significantly smaller than the cut-off scale: this scale could not be reached by the present epoch. The proper virial radii $r_v = x_v R / (1 + z_i)$ are few times larger for larger masses and in both cases agree well with the observational estimates of the sizes of the halos of galaxies and clusters.

The last two columns of Tables 2 and 3 give the concentrations c_{NFW1} and c_{NFW2} of the NFW formula. The values of c_{NFW1} were calculated from the model based on merging formalism provided by NFW that describes best the results of their N -body simulations, while c_{NFW2} are the values of concentration obtained by fitting formula (39) to the results of SIM. Following the arguments presented above the fits were done for the value of v calculated from the SIM. The width of the filter w was chosen so that the concentrations from NFW and SIM match for the smallest halos in the $n = -1$ case.

Figure 5 shows how the concentration c depends on the mass of the halo and the spectral index in the larger range of masses. The plots cover the largest range of mass available from SIM for different spectral indices with the initial conditions I adopted. The smallest masses were obtained for $z_i = 1500$ and the largest correspond to the point where the mass starts to decrease with z_i (the initial virial radii are then rather small, significantly smaller than the cut-off scale). The values of concentrations from the simulations were calculated in the same range of mass as the one obtained from SIM.

The solid lines give the concentrations obtained from fitting SIM results and the dashed lines are the N -body results of NFW (one has to remember that those curves are fits to points displaying some scatter that were themselves obtained by fitting the concentrations to the highly irregular density profiles of halos in the simulations). In each set the curves from top to bottom correspond to $n = 0, -0.5, -1$ and -1.5 respectively. The results for higher spectral indices

are shown in the smaller range of mass because obtaining halos of smaller mass for example in the case of $n = 0$ would require initial redshift of $z_i > 1500$ i.e. initial time earlier than the recombination epoch. Similar behaviour – more massive and more slowly forming halos for larger spectral indices – is observed in the N -body simulations of NFW. The two vertical dotted lines in the left panel indicate the mass scales chosen for detailed comparison shown in Figures 3-4 and Tables 2-3.

The left panel of Figure 5 shows the SIM results for the constant width of the cut-off filter $w = 0.6$ which matches the concentrations for smallest masses in the case of $n = -1$. There is however no reason why the same width of filter should apply for different spectral indices so we can try to adopt different widths for different spectral indices. Results of matching the SIM and NFW concentrations for the smallest masses in all cases are shown in the right panel of Figure 5. The adopted widths were $w = 0.14, 0.31, 0.6, 0.95$ respectively for $n = 0, -0.5, -1$ and -1.5 . Although we have no way of estimating the exact shape of the cut-off function from theory, one can expect that the cut-off will be sharper for peaks with sharper initial density distribution i.e. for higher spectral indices. This guess is in agreement with the dependence of the best matching values of w on the spectral index.

The predictive power of the improved SIM suffers also from the fact that the discrepancy between the SIM and NFW concentrations is much more sensitive to the unknown parameter w than to the cut-off scale, which we have estimated from the peaks formalism. Calculations of the profiles with different cut-off scales show that e.g. decreasing the cut-off scale gives smaller mass and steeper profile but because the mass is strongly affected the corresponding concentration from the simulations is also decreased and the factor by which both concentrations differ remains roughly the same.

On the other hand, decreasing the width of the cut-off filter does not significantly affect the mass while the concentration of SIM profiles is increased.

Leaving aside the exact determination of the width of the filter, Figure 5 proves that SIM predicts the same general trend in the dependence of the shape of dark halo profiles on their mass: the smaller the halo mass the steeper the profile. The dependence of the shape of the halo on the initial power spectrum is also reproduced in the wide range of masses: concentrations are larger for higher spectral indices up to a mass of the order of the nonlinear mass M_* where SIM approximation seems to break down. We can also conclude from Figure 5 that the agreement between SIM and the simulations is better for lower spectral indices. One may interpret this result as an indication that for spectra with more large scale power and long-distance correlations (low n) accretion is a realistic mechanism of growth of fluctuations. On the other hand, in the case of higher spectral indices isolated halos tend to appear and even relatively small halos form by merging of yet smaller objects.

Another argument for the reliability of SIM comes from the possible (and rather straightforward) application of the results presented here to more realistic scale-dependent power spectra. Since smaller masses correspond to smaller smoothing scales where the effective spectral index of a realistic spectrum is lower, the dependence of the concentration on mass according to the SIM should be flatter. This effect is also well visible in the simulations of NFW: for the CDM spectrum the trend of smaller concentrations with growing mass is preserved but the dependence on mass is rather weak (especially when we take into account large scatter in the results).

6 DISCUSSION

The improved SIM presented in this paper provides simple understanding of the dependence of the shape of the halo on its mass: smaller halos start forming earlier and by the present epoch their virial radii reach the cut-off scale that accounts for the presence of the neighbouring fluctuations; more massive halos form later and their virial radii are not affected by the cut-off scale, their virialized regions contain only the material that initially was quite close to the peak identified with the smoothing scale corresponding to the mass.

Although the concentrations of profiles predicted by SIM depend on the exact shape of the cut-off function, this study leads to rather firm conclusion that the agreement between the N -body and SIM profiles is the better the smaller the mass of the halo and the lower the spectral index of the initial power spectrum of fluctuations. If the profiles obtained from the simulations indeed reflect reality this may indicate that galactic halos form mostly by accretion, while for cluster size objects merging must be taken into account. As suggested by Syer & White (1998) the universal profile can be formed by sufficiently dense satellites reaching the centre of a halo intact and forming a cusp. Since the attempts to obtain the dependence of the profiles on mass only from formalisms describing the merging of halos (Nusser & Sheth 1999, Avila-Reese, Firmani & Hernandez 1998) have not been fully successful, it seems that the best descrip-

tion of halo profiles should be provided by a model dealing with a combination of accretion and merging (for the discussion on the distinction between the two phenomena see Salvador-Solé, Solanes & Manrique 1998). This work provides the understanding of the origin of universal profile in the case of small masses for which SIM can be considered a valid approximation.

One of the important shortcomings of SIM, that was not mentioned here, is the artificial combination of the linear and strongly nonlinear regime without taking into account the weakly nonlinear phase that may affect the initial density distribution before the strongly nonlinear evolution takes over. As discussed by Lokas (1998) these corrections are of similar importance as the ones introduced by using the formalism of BBKS to describe peaks in the density field instead of overdense regions. Both effects tend to steepen the initial density profiles but are difficult to model analytically (for the corrections for peaks see e.g. Ryden 1988). With the modifications of SIM introduced here we are interested mostly in regions not very distant from the centre of the forming halo. In these regions weakly nonlinear corrections to the expected overdensity $\langle \delta \rangle$ are known only numerically and it is difficult to obtain the cumulative density $\langle \Delta_i \rangle$. Even if we approximate it by some analytical expression we cannot proceed because the formula for the final profile is so complicated that any perturbative treatment is impossible. Qualitatively one may expect that the final profile will be somewhat steeper but since the value of $\Delta_{i,v}$ will not be changed the solution for the virial radius $x_{i,v}$ will be lower. It follows that also the halo mass will be decreased but it will have to be compared to a less massive and therefore steeper halo from the simulations, so it is difficult to predict whether the agreement between the two results would be improved. It should be added that this picture of weakly nonlinear corrections does not take into account the parallel evolution of the rms fluctuation σ itself. As discussed by Lokas et al. (1996) its value in the weakly nonlinear regime may be close to linear in the case of $n = -1$ but may differ significantly from the linear prediction for other spectral indices.

No solution to the problem of dark halo formation cannot be considered valid without a detailed agreement between its predictions and observations. To date several such comparisons were performed, in most cases in the form of fitting the NFW profile to the observed profiles of galaxies and clusters that are believed to be dominated by dark matter or provide some indication on how light traces mass. Carlberg et al. (1997) find that universal profile of NFW provides a very good fit to the density profiles of clusters in the CNOC survey, while Adami et al. (1998) find that galaxy distribution in clusters in the ENACS sample displays a core rather than a cusp in the central regions, but the mass distribution (Adami, private communication) is somewhat steeper. These results suggest that the universal profile indeed provides a good description of the density distribution in clusters. In the case of galaxies the situation is less satisfying. Kravtsov et al. (1998) analysed density profiles of dwarf and low surface brightness galaxies and found that they are much better fitted by a so-called Burkert profile (Burkert 1995) with a flatter cusp than in the NFW formula. They also performed a series of N -body simulations based on a different code than

that used by NFW and found similar shapes of galaxies as those observed.

ACKNOWLEDGMENTS

This work was supported in part by the Polish State Committee for Scientific Research grant No. 2P03D00815 and the French Ministry of Research and Technology within the program Jumelage (Astronomie Pologne). I wish to thank A. Mazure for his hospitality at Laboratoire d'Astronomie Spatiale in Marseille where part of this work was done.

REFERENCES

Adami C., Mazure A., Katgert P., Biviano A., 1998, A&A, 336, 63
 Avila-Reese V., Firmani C., Hernandez X., 1998, ApJ, 505, 37
 Bardeen J. M., Bond J. R., Kaiser N., Szalay A. S., 1986, ApJ, 304, 15 (BBKS)
 Burkert A., 1995, ApJ, 447, L25
 Carlberg R. G., Yee H. K. C., Ellingson E., et al., 1997, ApJ, L13
 Cole S., Lacey C., 1996, MNRAS, 281, 716
 Crone M. M., Evrard A. E., Richstone D. O., 1994, ApJ, 434, 402
 Efstathiou G., Frenk C. S., White S. D. M., Davis M., 1988, MNRAS, 235, 715
 Gott J. R., 1975, ApJ, 201, 296
 Gunn J. E., 1977, ApJ, 218, 592
 Gunn J. E., Gott J. R., 1972, ApJ, 176, 1
 Hoffman Y., Shaham J., 1985, ApJ, 297, 16 (HS)
 Katz N., Quinn T., Gelb J. M., 1993, MNRAS, 265, 689
 Kravtsov A. V., Klypin A. A., Bullock J. S., Primack J. R., 1998, ApJ, 502, 48
 Lacey C., Cole S., 1993, MNRAS, 262, 627
 Lokas E. L., Juszkiewicz R., Bouchet F. R., Hivon E., 1996, ApJ, 467, 1
 Lokas E. L., 1998, MNRAS, 296, 491
 Lokas E. L., 1999, in Hammer F. et al., eds, Proc. XXXIVth Rencontres de Moriond, Building the Galaxies. Editions Frontières, Gif-sur-Yvette, in press
 Navarro J. F., Frenk C. S., White S. D. M., 1997, ApJ, 490, 493 (NFW)
 Nusser A., Sheth R. K., 1999, MNRAS, 303, 685
 Padmanabhan T., Structure Formation in the Universe. Cambridge Univ. Press, Cambridge
 Peebles P. J. E., 1984, ApJ, 277, 470
 Quinn P. J., Salmon J. K., Zurek W. H., 1986, Nature, 322, 329
 Ryden B., 1988, ApJ, 333, 78
 Salvador-Solé E., Solanes J. M., Manrique A., 1998, ApJ, 499, 542
 Syer D., White S. D. M., 1998, MNRAS, 293, 337
 Tormen G., Bouchet F. R., White S. D. M., 1997, MNRAS, 286, 865
 Zaroubi S., Hoffman Y., 1993, ApJ, 416, 410

APPENDIX A: THE SCALE OF COHERENCE

The calculation of the scale of coherence $x_{i,coh}$ of the cumulative density contrast Δ_i can be done in a way analogous to the calculation of the scale of coherence x_{coh} of the density contrast δ itself (Lokas 1998). The condition for x_{coh} was

$$\langle \delta \rangle = \langle (\delta - \langle \delta \rangle)^2 \rangle^{1/2} \quad (A1)$$

where

$$\langle \delta \rangle = a\sigma\varrho \quad (A2)$$

$$\langle (\delta - \langle \delta \rangle)^2 \rangle = \sigma^2(1 - \varrho^2). \quad (A3)$$

The results were obtained from the two-point Gaussian probability distribution function for fields δ and γ , from which a conditional probability distribution for δ followed given that at distance r from where δ is measured there is an overdense region where the density is $\gamma = a\sigma$.

Here we may proceed in a similar fashion and consider a two-point probability distribution for variables Δ_i given by equation (7) and γ . If the condition for γ is the same we have (see also HS, Peebles 1984)

$$\langle \Delta_i \rangle = a\Sigma\varrho' \quad (A4)$$

$$\langle (\Delta_i - \langle \Delta_i \rangle)^2 \rangle = \Sigma_\Delta^2 = \Sigma^2(1 - \varrho'^2). \quad (A5)$$

The symbols Σ and Σ_Δ refer respectively to the unconstrained and constrained dispersions of the Δ_i field. The new correlation coefficient $\varrho' = \xi' / (\sigma\Sigma)$ is the normalized correlation function $\xi'(r_i) = \langle \Delta_i(r_i)\gamma(0) \rangle$.

The definition of Δ_i , equation (7), can be rewritten as

$$\Delta_i(r_i) = \frac{1}{(2\pi)^3} \int \delta(k) W_{TH}(kr_i) d^3k \quad (A6)$$

where $W_{TH}(kr_i)$ is the top-hat window function

$$W_{TH}(kr_i) = \frac{3[\sin(kr_i) - kr_i \cos(kr_i)]}{(kr_i)^3}. \quad (A7)$$

Expression (A6) leads to

$$\langle \Delta_i(r_i) \rangle = \frac{a}{(2\pi)^3 \sigma} \int P_R(k) W_{TH}(kr_i) d^3k \quad (A8)$$

where $P_R(k)$ is the power spectrum initially smoothed with the Gaussian filter (2)

$$P_R(k) = P(k) e^{-k^2 R^2}. \quad (A9)$$

The expected cumulative density is therefore

$$\langle \Delta_i \rangle = \frac{6Ca}{(2\pi)^2 r_i^{n+3} \sigma} I_1(x_i) \quad (A10)$$

where

$$\begin{aligned} I_1(x_i) &= \int_0^\infty k^{n-1} (\sin k - k \cos k) e^{-k^2/x_i^2} dk \\ &= \frac{1}{2} x_i^{n+1} \Gamma\left(\frac{n+1}{2}\right) \left[{}_1F_1\left(\frac{n+1}{2}, \frac{3}{2}, -\frac{x_i^2}{4}\right) \right. \\ &\quad \left. - {}_1F_1\left(\frac{n+1}{2}, \frac{1}{2}, -\frac{x_i^2}{4}\right) \right] \end{aligned} \quad (A11)$$

Together with the expression for σ , equation (4), this leads to the expression (14) for the expected cumulative density.

The unconstrained variance of Δ_i is

$$\Sigma^2 = \frac{1}{(2\pi)^3} \int P_R(k) W_{TH}^2(kr_i) d^3k = \frac{18C}{(2\pi)^2 r_i^{n+3}} I_2(x_i) \quad (A12)$$

where

$$\begin{aligned}
 I_2(x_i) &= \int_0^\infty k^{n-4} (\sin k - k \cos k)^2 e^{-k^2/x_i^2} dk \quad (\text{A13}) \\
 &= \frac{1}{2} x_i^{n-3} \Gamma\left(\frac{n-1}{2}\right) \left[\frac{x_i^2+2}{2} {}_1F_1\left(\frac{n-1}{2}, \frac{1}{2}, -x_i^2\right) \right. \\
 &\quad \left. - \frac{n-2}{n-3} {}_1F_1\left(\frac{n-3}{2}, \frac{1}{2}, -x_i^2\right) + \frac{x_i^2}{2} + \frac{1}{n-3} \right]
 \end{aligned}$$

and the correlation coefficient is given by

$$\varrho'^2 = \frac{2}{\Gamma[(n+3)/2]} x_i^{-(n+3)} \frac{I_1^2}{I_2}. \quad (\text{A14})$$

Given the analytical expressions for $\langle \Delta_i \rangle$, Σ and ϱ' equation (15) has to be solved numerically to determine $x_i = x_{i,\text{COH}}$. The results for different power spectra are shown in Figure 1.